Geophys. J. Int. (1992) **110**, 283–296

Shear waves from three-component ocean bottom seismographs off Lofoten, Norway, indicative of anisotropy in the lower crust

Rolf Mjelde

Institute of Solid Earth Physics, Allégt. 41, University of Bergen, 5007 Bergen, Norway

Accepted 1992 February 7. Received 1992 February 4; in original form 1991 April 8

SUMMARY

Data from four three-component ocean bottom seismographs (OBS) situated on a 145 km long profile on the Røst High on the continental shelf off Lofoten, northern Norway, have been modelled using 2-D seismic ray tracing, and a *P*- and *S*-wave velocity model along the profile is presented. The *S*-wave model has been obtained from a study of the high quality, horizontal component data.

A V_P/V_S ratio of 1.95–2.15 is found in the sedimentary layers on the Røst High. These high values are consistent with shaly sediments, which are identified in dredged bedrock samples. South of the Røst High a considerably lower V_P/V_S ratio (ca. 1.6) is estimated for the sediments, which can be attributed in part to a higher degree of compaction in the deepest sediments and in part to a more sandy lithology.

In the upper and middle crystalline crust a V_P/V_S ratio of 1.75 is obtained. Strong *S* reflections and *P*-to-*S* conversions at the Moho are observed on all four instruments, and the modelling of these arrivals indicates that the *S*-wave velocity in the lower crust varies with angle of incidence, from 3.5 km s^{-1} ($V_P/V_S = 1.95$) at vertical incidence to 4.0 km s^{-1} ($V_P/V_S = 1.7$) at 60–70°. This angle of incidence dependent *S*-wave anisotropy (the order of 10 per cent) is consistent with some horizontal or subhorizontal layering in the lower crust.

Key words: anisotropy, lithology, 3-C OBS, V_P/V_S ratio.

1 INTRODUCTION

Seismic refraction and reflection studies of sedimentary and crustal structures have generally been restricted to *P*-waves. The main reason for omitting *S*-waves from the data analysis has been the lack of three-component data.

During the last two decades interest in *S*-waves has, however, been steadily increasing. This is partly due to the higher quality data obtained with improved acquisition technology, often with use of three-component seismometers, and partly due to the recognition that *S*-waves can give important information about rock parameters not achievable through the study of *P*-waves alone. Knowing the *P*-wave velocity only offers restricted possibilities to constrain the lithology, whereas knowing both *P*-wave velocity (V_P) and *S*-wave velocity (V_S) enables the calculation of the V_P/V_S ratio which is sensitive for instance to the quartz and feldspar content (Christensen & Fountain 1975; Kern 1982) and the presence of fluids (Nur & Simmons 1969; Spencer & Nur 1976; Christensen 1984).

Another interesting aspect of *S*-waves is their sensitivity to the orientation of cracks and microcracks documented through numerous observations of *S*-wave splitting (Crampin 1990), and their possible sensitivity to preferred orientations of minerals and grains.

Numerous attempts to incorporate *S*-waves in crustal studies have been performed, e.g. Sellevoll & Pomeroy (1968); Braile *et al.* (1974); Kanestrøm & Johnstad (1975); Assumpcao & Bamford (1978); Gajewski (1981); Hall & Ali (1985); Kullinger & Lund (1986); Holbrook, Gajewski & Prodehl (1987); Holbrook *et al.* (1988); Chroston & Brooks (1989); Gajewski *et al.* (1990); Goodwin & McCarthy (1990).

The oil industry has shown increased attention to *S*-waves due to the reasons mentioned above, and also the possibility that combined *P*- and *S*-wave velocities offer to distinguish between gas saturated and water saturated rock (Ostrander 1984).

In this study a two-dimensional *P*- and *S*-wave velocity model along a profile shot on the Røst High on the continental shelf off Lofoten, northern Norway is presented. The profile was part of an extensive survey performed in

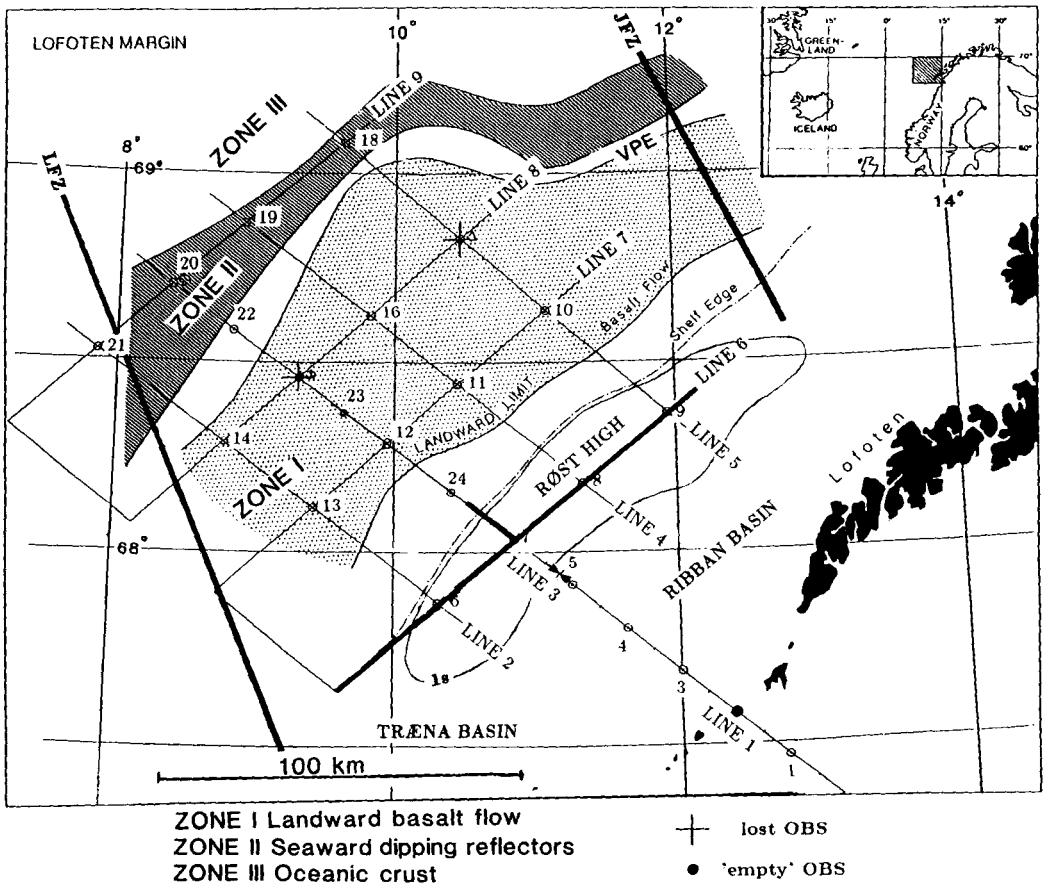

Figure 1. Main structural elements off Lofoten with position of OBS units and seismic reflection lines shot during the 1988 survey indicated. Line 6, described in this paper, and the location (on line 3) of the reflection profile shown in Fig. 14, are indicated with heavy lines. VPE—the northward continuation of the Vøring escarpment; LFZ—Lofoten Fracture Zone; and JFZ—Jennegga Fracture Zone. 1s = two-way traveltime to the base Cretaceous reflector (from reflection seismics). Modified from Sellevoll (1988).

1988 September using twenty four 3-C ocean bottom seismographs (OBS) (Fig. 1). The data from the profile contain considerable *S*-wave energy converted from *P*-waves, probably at the sea-floor.

2 GEOLOGICAL FRAMEWORK

The region (Fig. 2) was, in the late Silurian to early Devonian, characterized by a compressional regime, resulting in suturing of the North American/Greenland and the Eurasian/Fennoscandian plates and the formation of the Caledonides (Bukovics *et al.* 1984; Bøen, Eggen & Vollset 1984; Gage & Dore 1986).

The margin has been dominated by extensional tectonics in post-Caledonian time. The late Jurassic/early Cretaceous extensional episode was the most important leading to strong differential subsidence and the formation of the main structural elements. The entire Arctic–north Atlantic rift system was reactivated in the early Tertiary, resulting in sea-floor spreading between the North American/Greenland and Eurasian plates.

The Røst High, situated on the continental shelf off Lofoten, is a complex northeast–southwest trending basement high causing distinct positive gravimetric and magnetic anomalies. Its termination to the south and north coincides with the landward projection of the Lofoten and Jennegga fracture zones respectively (Mokhtari & Pegrum 1991, fig. 1).

The gross morphology of the Røst High suggests that it is the crest of a southeastward rotated fault block complex generated during the late Jurassic/early Cretaceous extensional episode (Mokhtari & Pegrum 1991; Fig. 3). Based on the study of sparker profiles and bedrock sampling the thin sedimentary cover is inferred to be mainly Cretaceous in age, with smaller local amounts of older Mesozoic sediments (Rokoengen & Sættem 1983; Løseth *et al.* 1989). Any Tertiary cover has been removed by uplift and erosion.

The crystalline basement in Lofoten (Fig. 1) is believed to represent an exhumed deep section of the crust (Chroston & Brooks 1989). Within the Lofoten archipelago Archaean and Proterozoic rocks lie within a belt of basement gneisses to the west of the Caledonian nappes. The Lofoten suite comprises high-grade metamorphic rocks of granulite and amphibolite facies. The crystalline basement on the Røst High might be similar to the crust observed within Lofoten, or it might represent a shallower part of the crust that has been eroded in Lofoten.

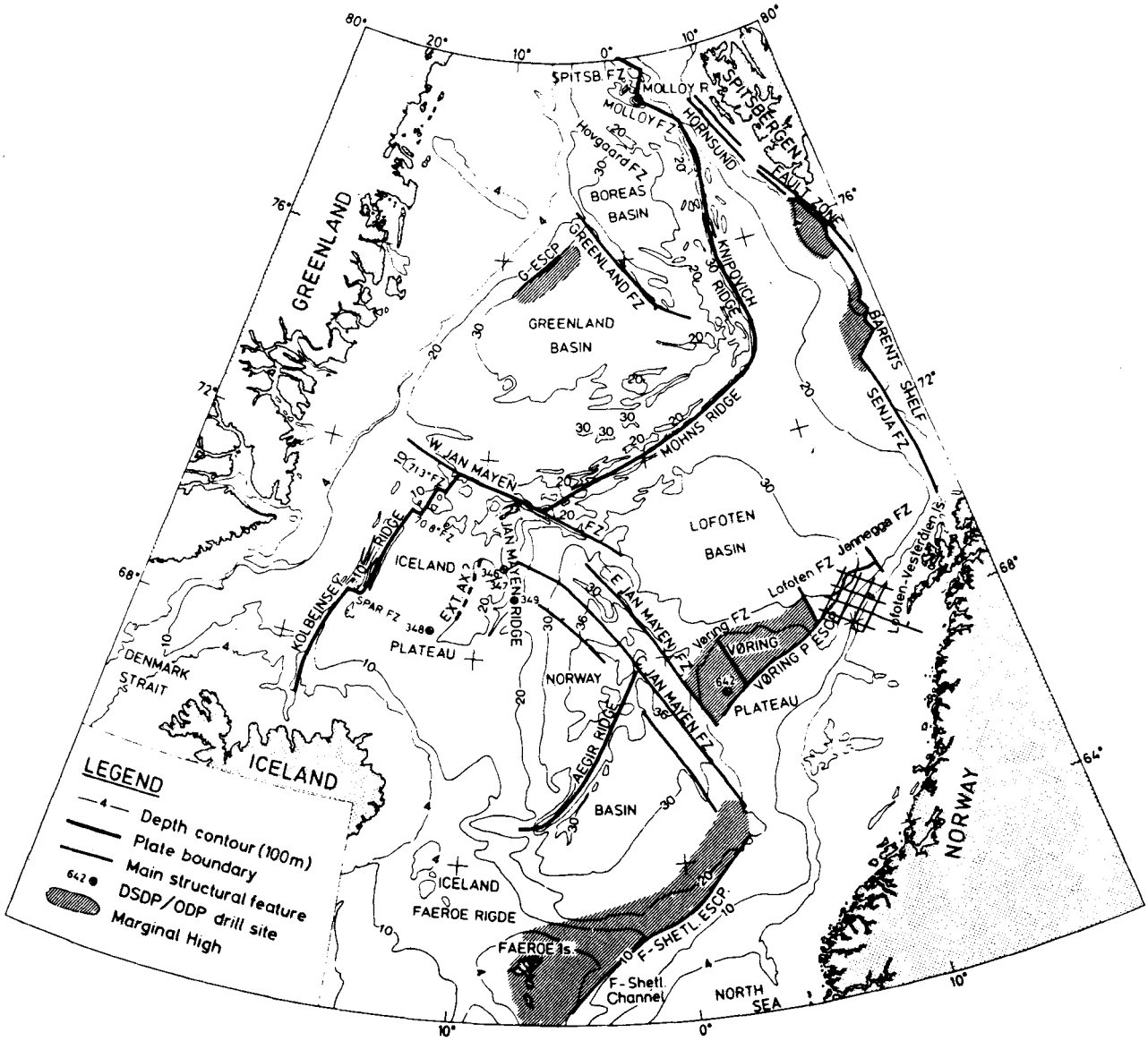

Figure 2. Regional physiography and structural features of the ocean basins and continental margins in the Norwegian–Greenland Sea. Also indicated ODP drill site 642 and profiles shot in 1988. Modified from Eldholm *et al.* (1990).

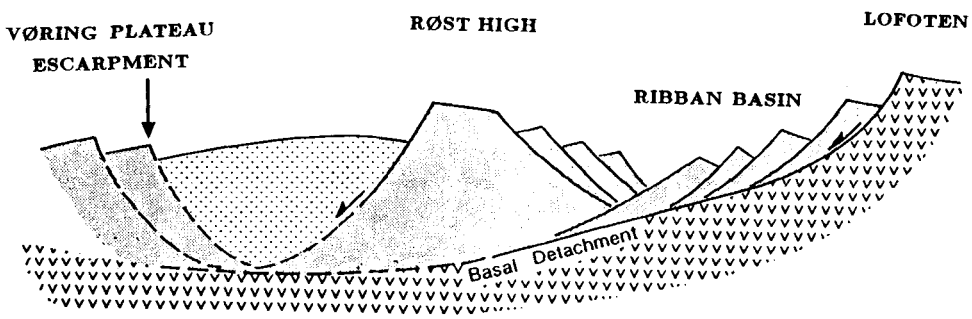

Figure 3. Main structural elements (schematic) along a profile perpendicular to Lofoten. After Mokhtari (1991).

3 DATA ACQUISITION

The acquisition of the seismic refraction data was performed from 1988 July 29 to August 19 using R/V Håkon Mosby, University of Bergen. The data acquisition was performed in cooperation between the Institute of Solid Earth Physics (Seismological Observatory), University of Bergen, the Laboratory for Ocean Bottom Seismology, Hokkaido University and the Geophysical Institute, University of Tokyo.

The scientific programme comprised seismic reflection, seismic refraction and gravimetric measurements. Fig. 1 shows the most important geological features in the investigated area with the position of the seismic reflection lines and OBS units indicated. The study described in this paper is limited to profile 6 (Fig. 1).

Four Bolt C air-guns with a total volume of 78.7 l (4800 in^3) were used as source. The depth of the air-guns was about 21 m, and one shot was fired every 2 min. Thus the distance between each shot was ≈240 m. The effective length of the streamer was 1950 m.

Four OBS at about 30 km intervals were used to acquire the seismic refraction data along the profile studied. These instruments were developed and built by the geophysical institutes at Hokkaido and Tokyo Universities. The analogue OBS instruments have three orthogonal components (4.5 Hz gimbal mounted geophones); one vertical and two horizontal. The instruments can record continuously for 14 days within the frequency range from 1 to 30 Hz (−3 dB).

4 DATA PROCESSING

The OBS data were digitized at Hokkaido and Tokyo Universities, and further processed at the University of Bergen.

A typical OBS frequency spectrum shows that the seismic signals (both *P*- and *S*-wave arrivals) contain most energy

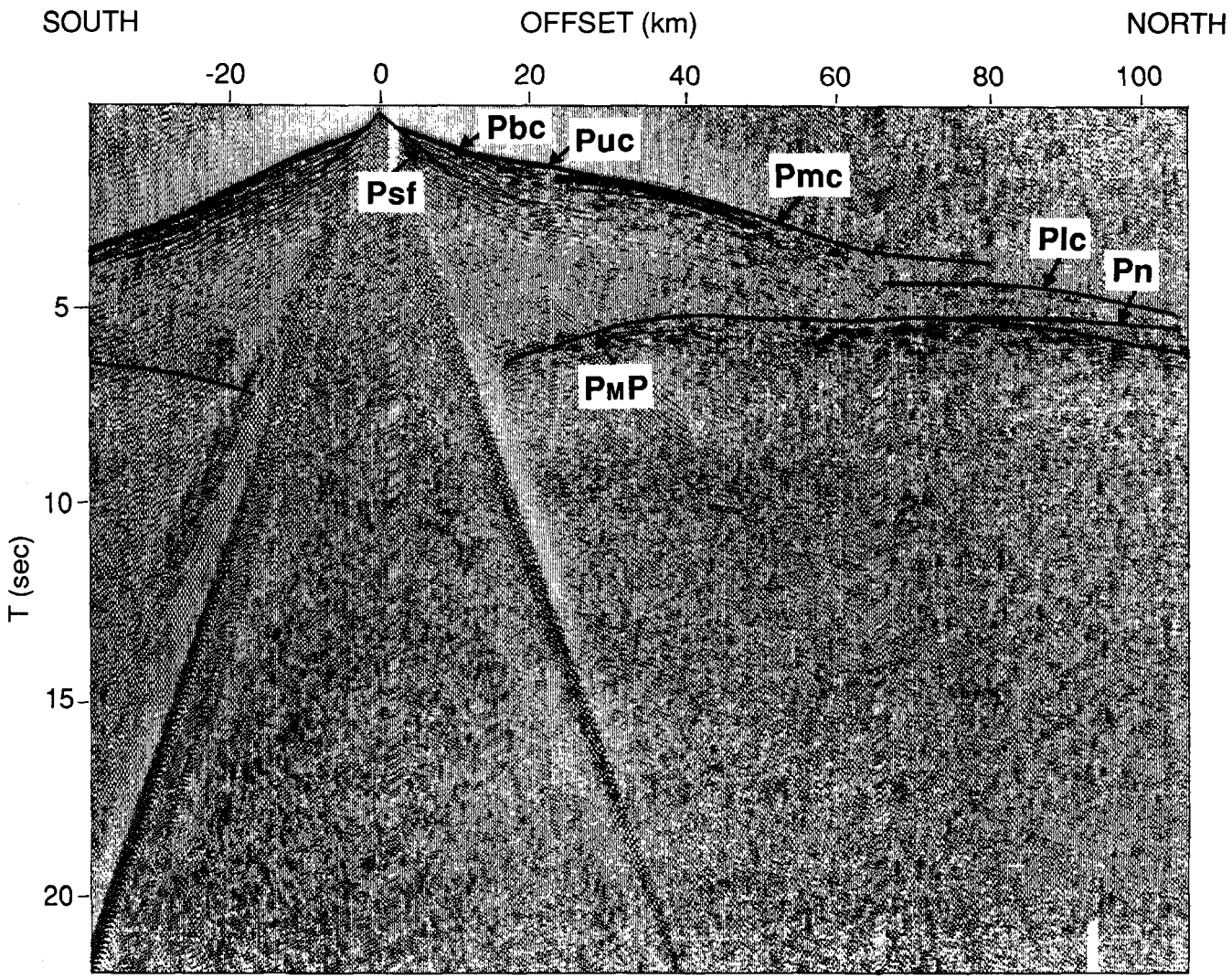

Figure 4. OBS 6 vertical component (reduction velocity 8.0 km s^{-1}, 6–13 Hz band-pass filtered, deconvolved.) P_{sf}—sea-floor refraction; P_{bc}—base Cretaceous refraction; P_{uc}—upper crust refraction; P_{mc}—middle crust refraction; P_{lc}—lower crust refraction; P_n—Moho refraction; and P_MP—Moho reflection.

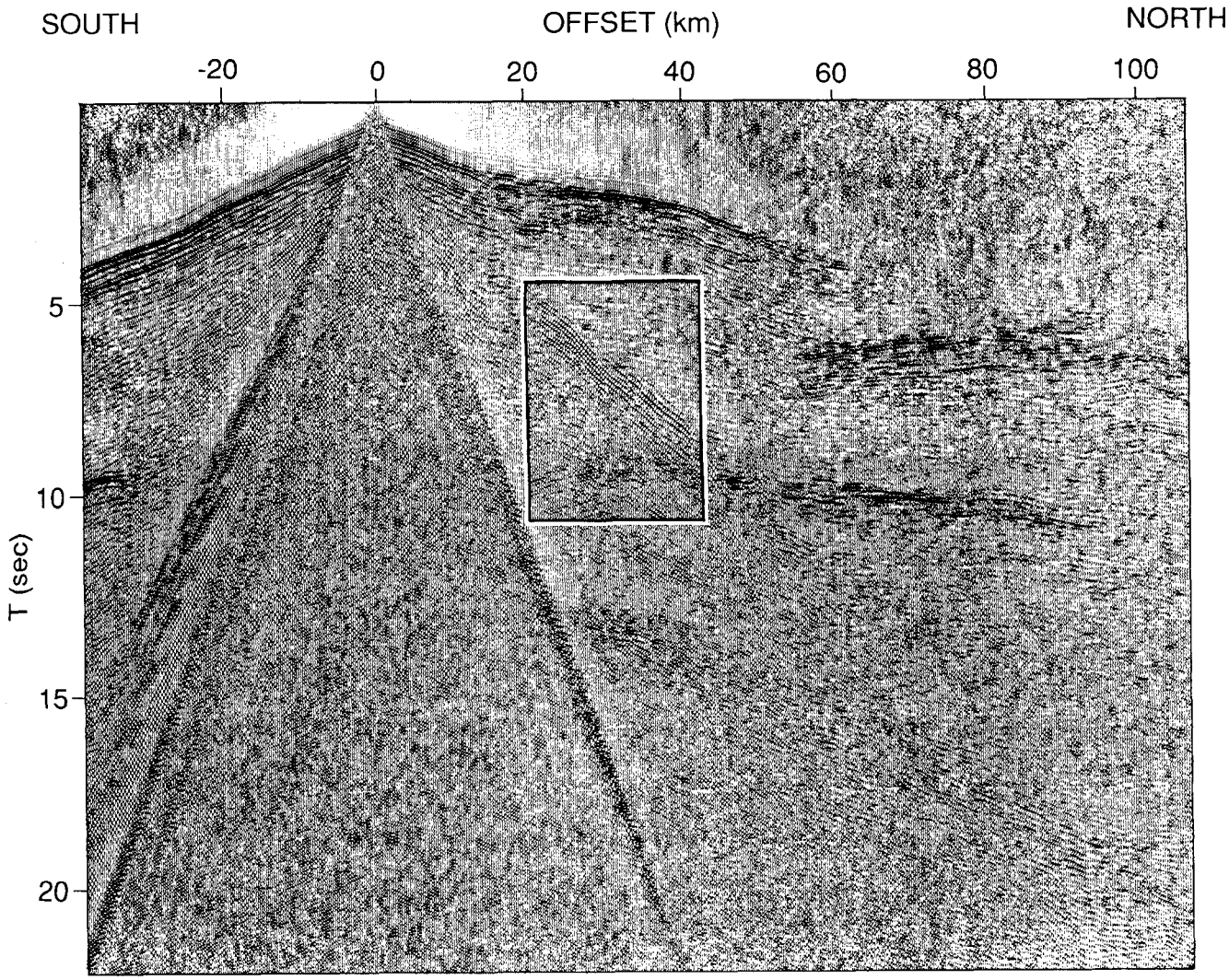

Figure 5. OBS 6 horizontal component (reduction velocity 8.0 km s^{-1}, 6–13 Hz band-pass filtered, deconvolved.) A close-up of the framed part is shown in Fig. 6.

between ca. 6 and 13 Hz, which is higher than the main energy in the noise spectrum (ca. 1–3 Hz) (Mjelde *et al.* 1991).

Both the vertical and horizontal components of the OBS data recorded during the Lofoten experiment are of very high quality, which simplified the processing in that only band-pass filtering (6–13 Hz) was required in the preliminary modelling of the *P*-waves (Mjelde *et al.* 1991).

The *S*-waves have, however, poorer signal-to-noise ratio, and the data were thus processed further before the *S*-waves observed on the Røst High were modelled. The first step in this processing consisted of applying a velocity filter to the data to remove the noise caused by the time-signal (one pulse every second registered on a separate channel) (Fig. 9). In addition, velocity-filters were used to help identification of the different *S*-wave phases. The data were then deconvolved using a spiking deconvolution operator with 1500 ms length. Fig. 5 shows the OBS 6 seismogram after deconvolution and removal of the time-signal. The signal/noise ratio of the S_{uc} and S_{mc} phases (upper and middle crust, see Fig. 6) has improved considerably after the processing. All data presented in this paper have been processed like the OBS in Fig. 5 unless otherwise specified. The data are plotted with Automatic Gain Control (4 s window) and displayed with traveltime reduced with a velocity of 8 km s^{-1}, except Fig. 8 which shows the data from OBS 7 before reduction.

5 MODELLING AND DISCUSSION

The OBS data have been modelled using 2-D ray tracing software developed under a joint project between the University of Bergen and the Norsk Hydro Research Centre in Bergen. Constant-velocity layers have been assumed in the models, and only kinematic (traveltime) modelling has been performed.

Figs 4–12 show seismograms, after processing as described above, from two vertical components (high gain; OBS 6 and 7) and from one of the horizontal components (high gain) from the four OBS investigated. Calculated

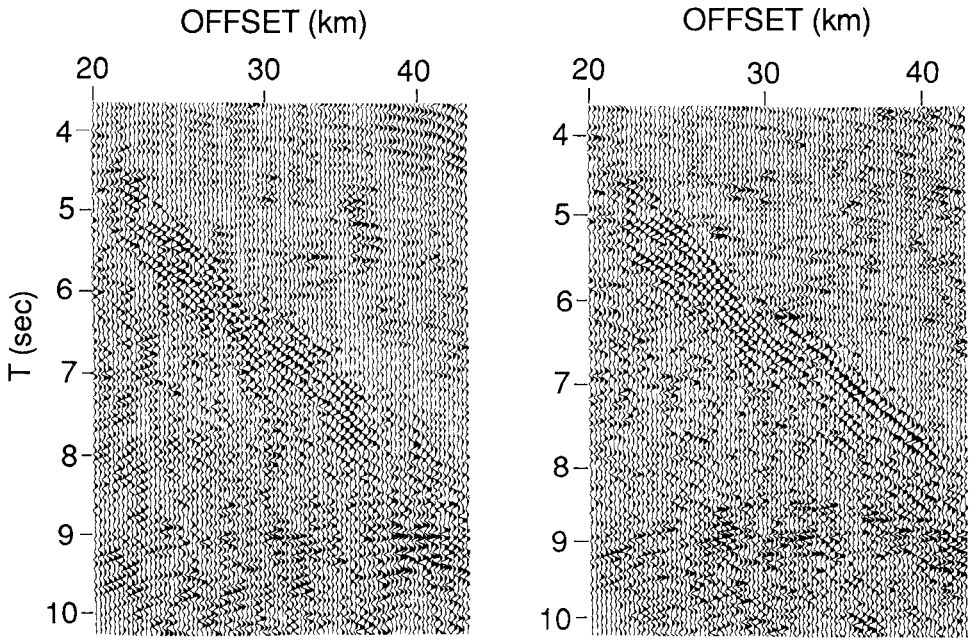

Figure 6. Close-up of part of the seismogram shown in Fig. 5 demonstrates the effectivness of the deconvolution filter applied. Left-hand side before deconvolution, and right-hand side after deconvolution.

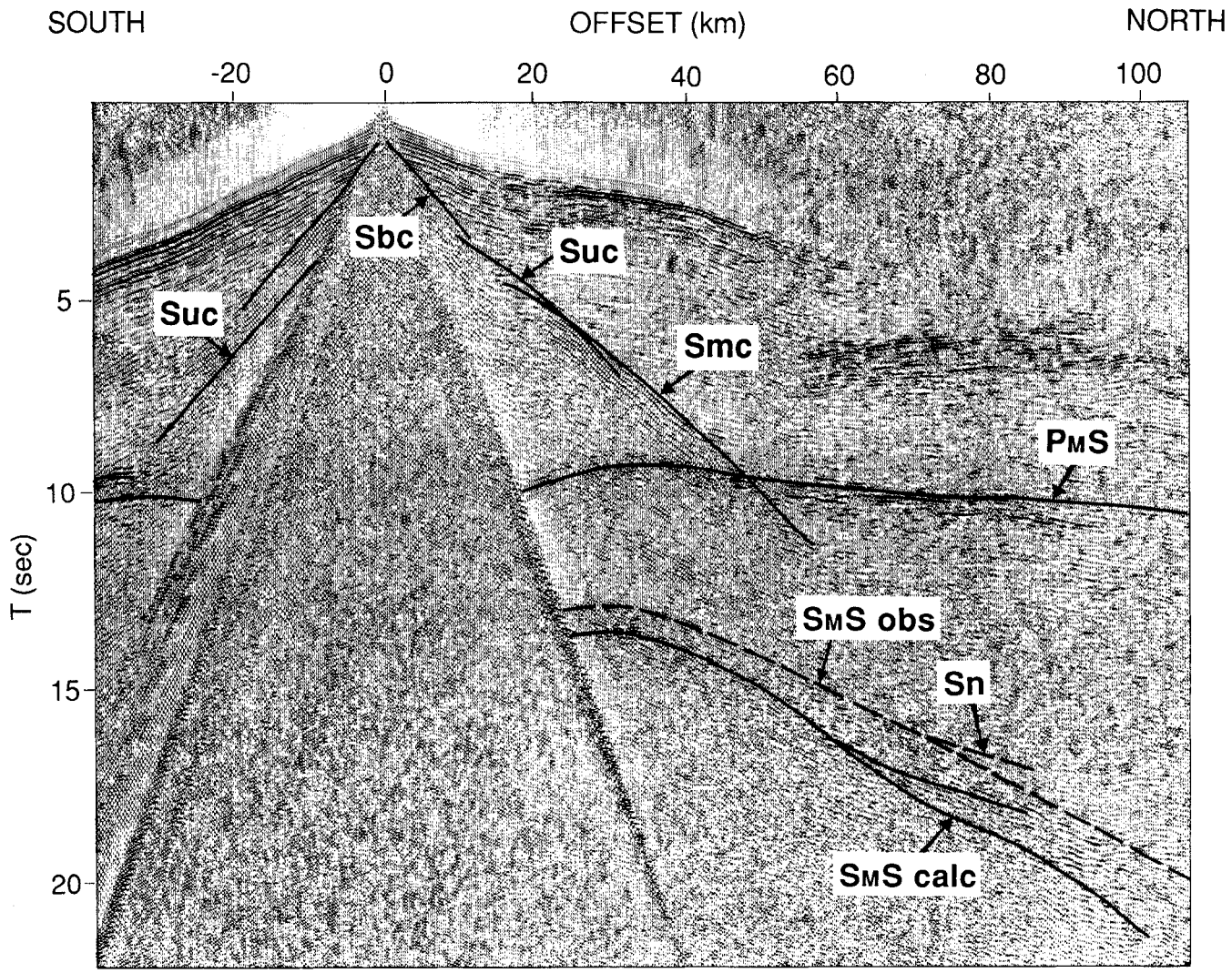

Figure 7. OBS 6 horizontal component (reduction velocity 8.0 km s^{-1}, 6–13 Hz band-pass filtered, deconvolved.) S_{bc}—base Cretaceous refraction; S_{uc}—upper crust refraction, S_{mc}—middle crust refraction; S_n—Moho refraction; S_MS—Moho reflection; and P_MS—mode conversion at Moho. Hatched and heavy lines represent observed and calculated traveltime curves respectively.

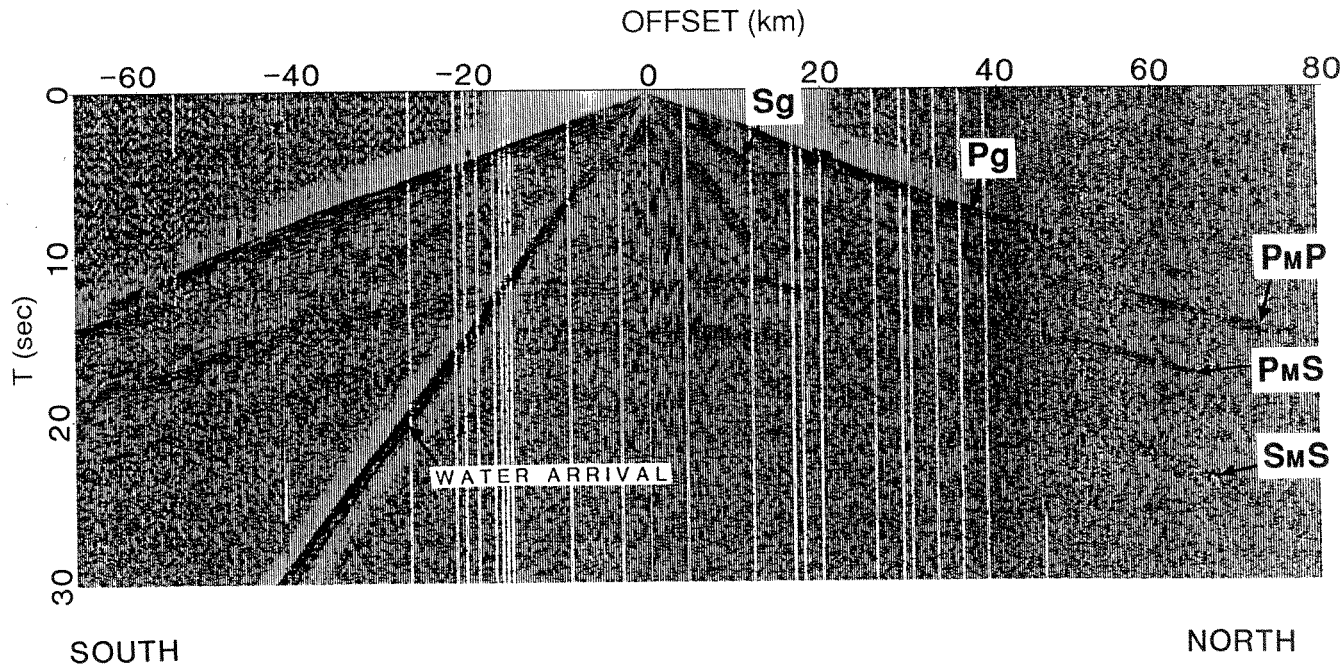

Figure 8. OBS 7 horizontal component (6–13 Hz band-pass filtered.)

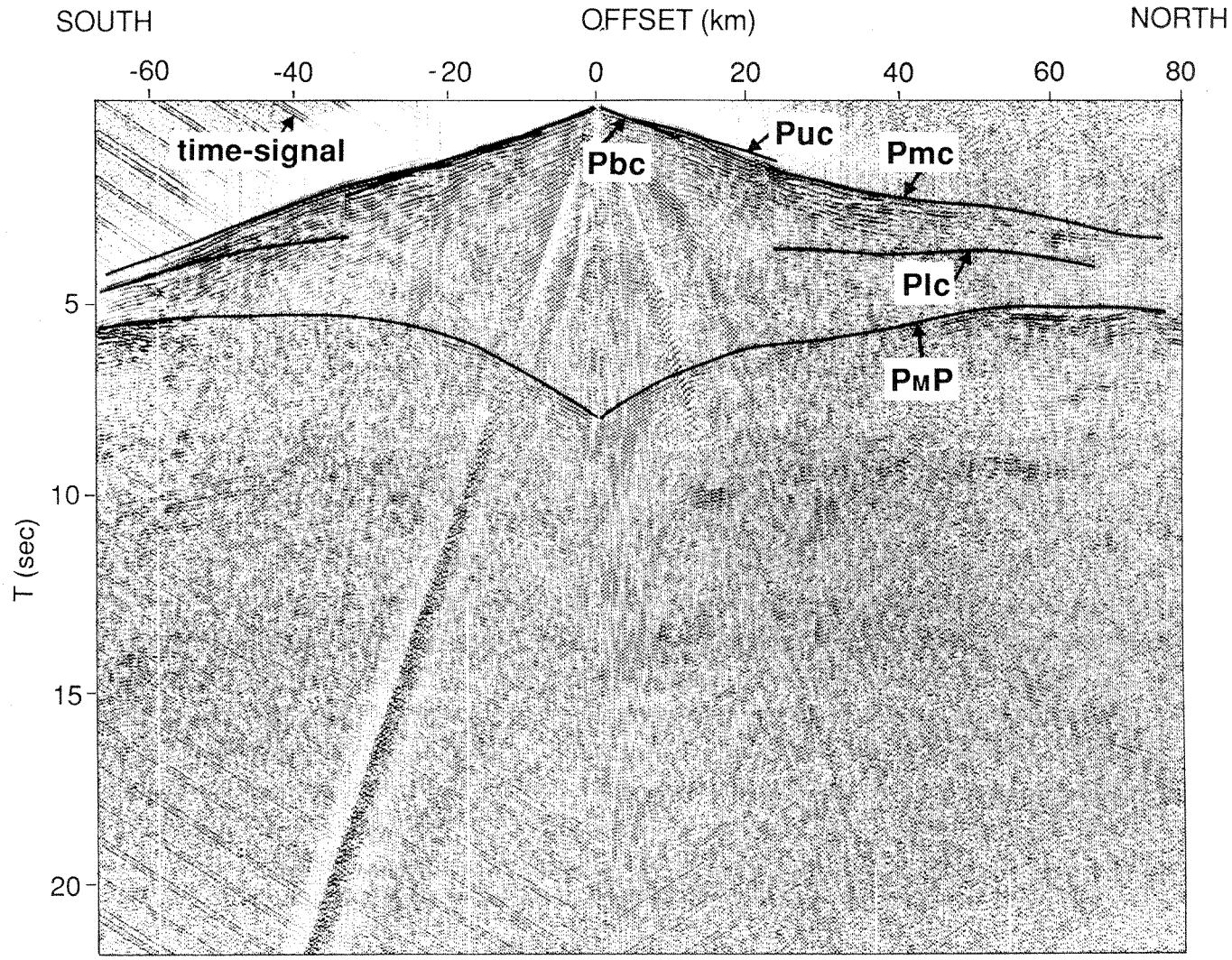

Figure 9. OBS 7 vertical component (reduction velocity 8.0 km s^{-1}, 6–13 Hz band-pass filtered.) P_{bc}—base Cretaceous (sea-floor) refraction; P_{uc}—upper crust refraction; P_{mc}—middle crust refraction; P_{lc}—lower crust reflection; and $P_M P$—Moho reflection.

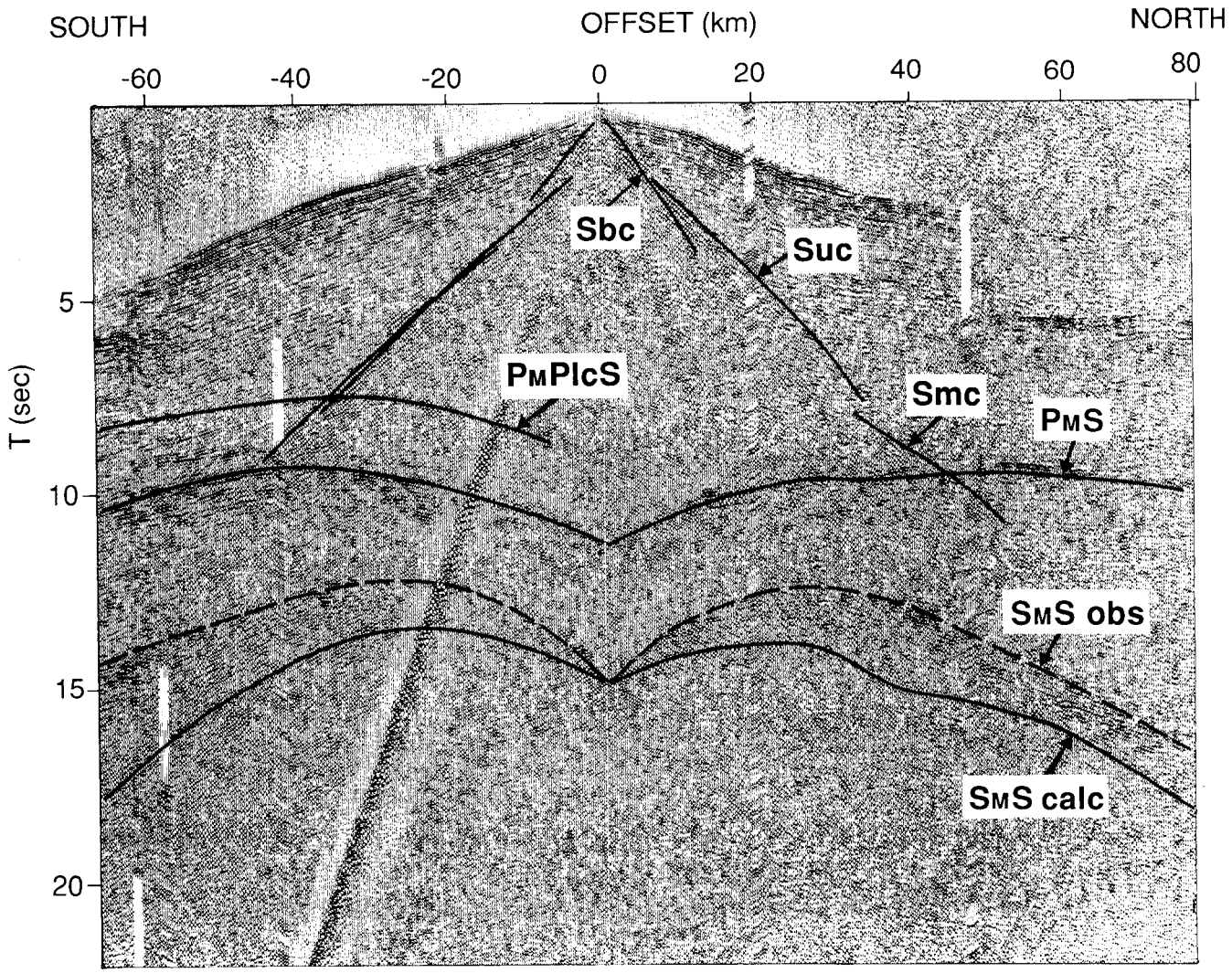

Figure 10. OBS 7 horizontal component (reduction velocity 8.0 km s^{-1}, 6–13 Hz band-pass filtered, deconvolved.) S_{bc}—base Cretaceous refraction; S_{uc}—upper crust refraction; S_{mc}—middle crust refraction; $P_M P_{lc} S$—mode conversion at the top of the lower crust; $S_M S$—Moho reflection; and $P_M S$—mode conversion at Moho. Hatched and heavy lines represent observed and calculated traveltime curves respectively.

traveltimes indicated in the figures represent critical refractions (head waves) plotted from the critical angle, unless otherwise specified in the figures. Only one of the horizontal components is presented since the two (non-reoriented) horizontal components are apparently very similar. The relatively low quality of the *S*-wave arrivals on the vertical component seismograms (Figs 4 and 9) indicates that the *S*-waves can only be interpreted and modelled in a reliable way by studying the horizontal components. The important $S_M S$ phase, for instance, is observed clearly only on the horizontal components.

5.1 The *P*-wave model

The 2-D *P*- and *S*-wave velocity models for the profile are presented in Fig. 13. We estimate the uncertainty in the Moho depth to be ±1 km and in the velocities ±0.1 km s^{-1}. A more detailed uncertainty analysis is described in Mjelde *et al.* (1991).

The area is characterized by high *P*-wave velocities close to the sea-floor. The sea-floor velocity is estimated to be 3.1 km s^{-1}, but close to OBS 7 a velocity as high as 5.1 km s^{-1} is measured. The 5.1 km s^{-1} refractor coincides with the base Cretaceous reflector interpreted by Mokhtari, Pegrum & Sellevoll (1989). The high velocities indicate that sequences of Mesozoic and Cenozoic sediments are absent or very thin (thickness below the resolution of the *P*-wave) close to OBS 7.

The 6.0 km s^{-1} refractor is interpreted as the top of crystalline basement. Langnes (Statoil, personal communication) found that this refractor corresponds to the top of magnetic basement in this area, an observation that supports the interpretation. The crystalline crust is divided into three layers; an upper, an intermediate and a lower crustal layer with velocities of 6.0, 6.4 and 6.8 km s^{-1} respectively. The interfaces between these layers can be interpreted as first-order discontinuities on at least one OBS (Mjelde *et al.* 1991). The velocities found correspond in general with earlier studies (Sellevoll 1973; Sellevoll & Thanvarachorn 1977; Drivenes *et al.* 1984).

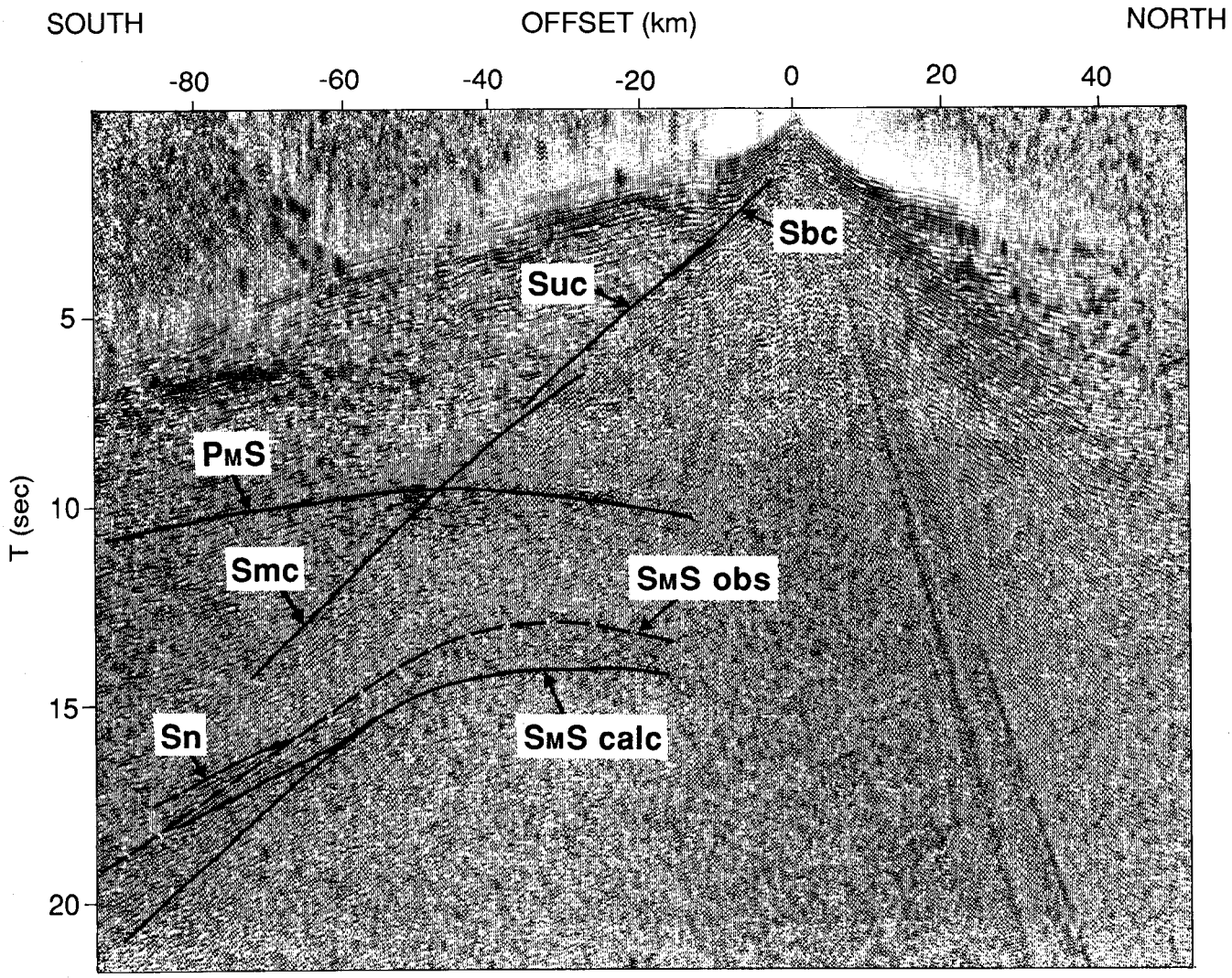

Figure 11. OBS 8 horizontal component (reduction velocity 8.0 km s^{-1}, 6–13 Hz band-pass filtered, deconvolved.) S_{bc}—base Cretaceous refraction; S_{uc}—upper crust refraction; S_{mc}—middle crust refraction; S_n—Moho refraction; S_MS – Moho reflection; and P_MS—mode conversion at Moho. Hatched and heavy lines represent observed and calculated traveltime curves respectively.

5.2 The *S*-wave model in the sediments

The *P*-wave model, which is described in detail in Mjelde *et al.* (1991), was used as a basis for modelling the *S*-waves. The *S*-wave velocities that best satisfy the observations are indicated in Fig. 13. It has been assumed that the waves are *P*-to-*S* converted at the sea-floor, which represents by far the highest impedance contrast. The other impedance contrasts in the model are artificially high since the model consists of relatively few, constant velocity layers.

The *S*-wave velocity in the shallow sedimentary layer (post-Jurassic) is estimated by use of the intercept time for the critical refraction along the top of the deep sedimentary layer (pre-Cretaceous; S_{bc}). The modelling indicates a V_P/V_S ratio of 2.15 ($V_S = 1.4$ km s^{-1}) in the shallow layer, and a V_P/V_S ratio of 1.95 ($V_S = 2.6$ km s^{-1}) in the deep layer.

The V_P/V_S ratio in several different sedimentary sequences has been shown to be related to the sand/shale ratio; a V_P/V_S ratio of 1.6 representing sand and a V_P/V_S ratio of 2.0 representing shale (Neidell 1985). If the sedimentary layers on the Røst High consist mainly of sand and shale, one might hence infer from the esimated V_P/V_S ratios that the layers consist of much more shale than sand. This interpretation is supported by dredged bedrock samples from this area which indicate that the sediments ranging from lower Cretaceous to Paleocene in age are uniform and consist mainly of claystone (Løseth *et al.* 1989). The consistency between estimated V_P/V_S ratio and observed lithology supports the assumption that *P*-to-*S* conversions occur at the sea-floor.

South of the Røst High where the layers dip steeply towards the Træna Basin, the *S* phases arrive earlier than predicted when the above mentioned *S*-wave velocities are used in the sedimentary layers. This can in part be attributed to the increased compaction of the deepest sediments in this area. Incorporating a V_P/V_S ratio of 1.6 ($V_S = 1.9$ and 3.2 km s^{-1} for the two layers) below 3 km depth (the depth to crystalline basement on the Røst High), which should more than compensate for the higher degree

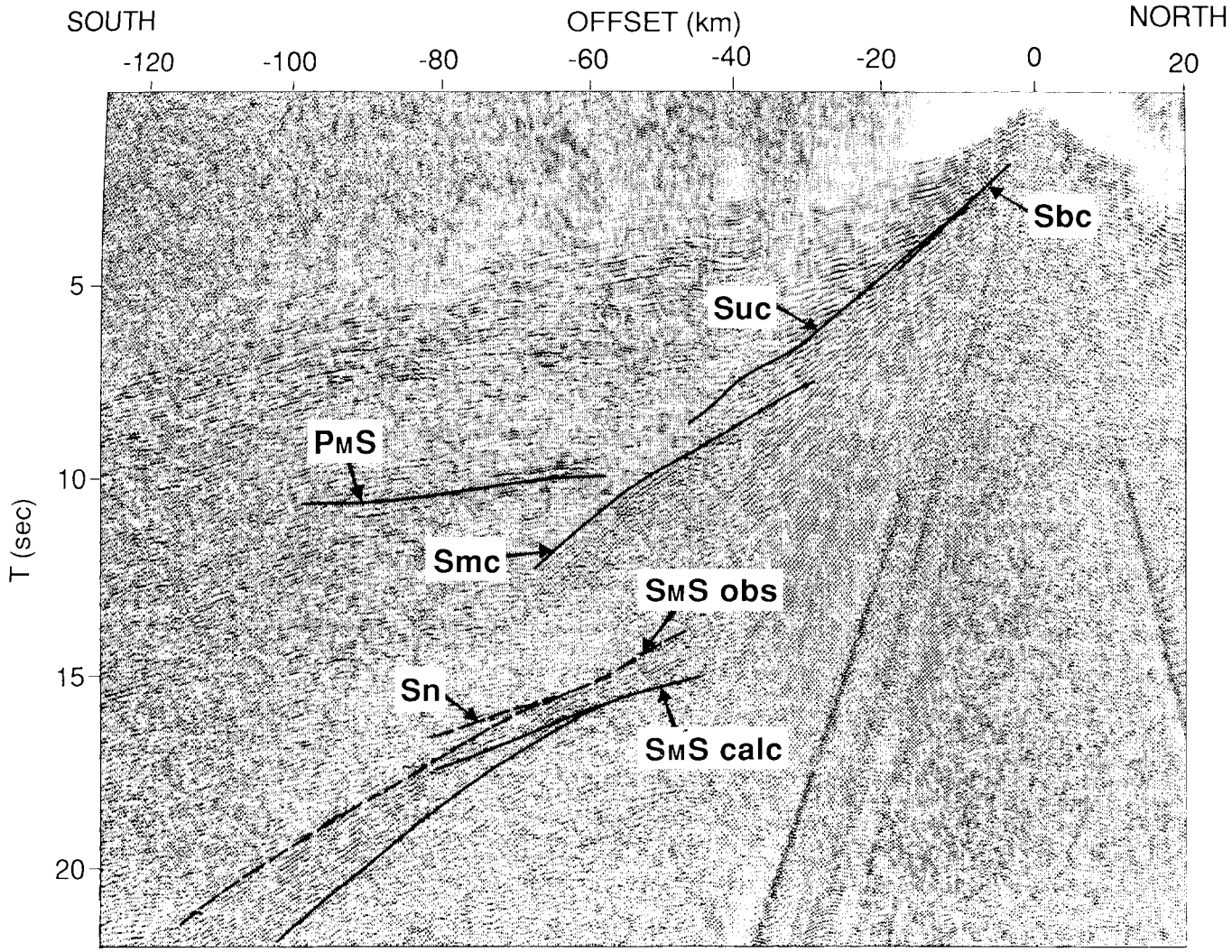

Figure 12. OBS 9 horizontal component (reduction velocity 8.0 km s^{-1}, 6–13 Hz band-pass filtered, deconvolved.) S_{bc}—base Cretaceous refraction; S_{uc}—upper crust refraction; S_{mc}—middle crust refraction; S_n—Moho refraction; S_MS—Moho reflection; and P_MS—mode conversion at Moho. Hatched and heavy lines represent observed and calculated traveltime curves respectively.

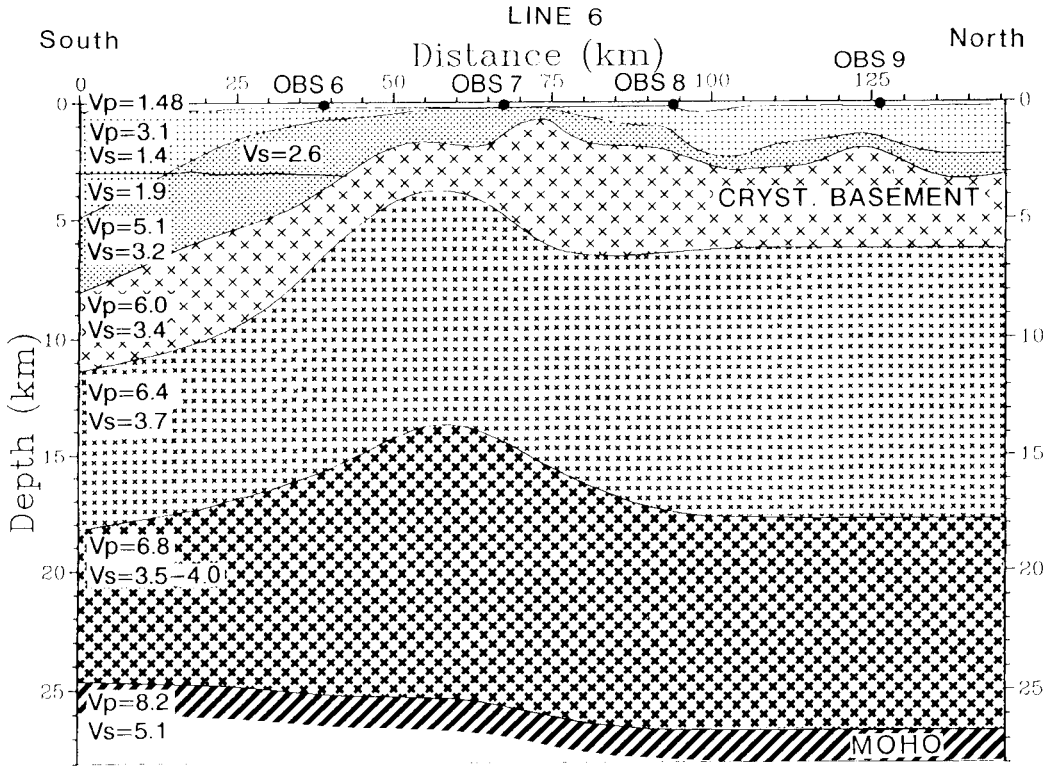

Figure 13. *P*- and *S*-wave velocity model of line 6.

of compaction, gives a much better fit to the observations (see Figs 7 and 10). The *S*-waves seem, however, to arrive slightly earlier than predicted even by this model [see the P_MS arrival on OBS 6 (southern side; Fig. 7)]. This indicates that the *S*-wave velocity in the sedimentary layers, also above about 3 km depth, is higher in this area than on the Røst High, which might indicate that the sediments contain more sand south of the High. No bedrock samples have yet been collected in this area, but interpretation of shallow seismic reflection data indicates that the sediments are more complex than on the Røst High (Løseth *et al.* 1989), which might indicate that they may contain significant amounts of sand. The discussion below concerning the lower crust will show, however, that extreme care must be taken in relating the V_P/V_S ratio to lithology.

5.3 The *S*-wave model in the crystalline crust

The V_P/V_S ratio in the upper and middle crystalline crust is found to be 1.75 ($V_S = 3.4$ and 3.7 km s^{-1} respectively).

The seismograms (Figs 7, 10–12) show that the *S*-wave reflection from Moho S_MS deviates strongly from that predicted from the model. The modelling of the S_MS phase on OBS 7 shows that a V_P/V_S ratio of 1.95 ($V_S = 3.5$ km s^{-1}) satisfies the observations for waves propagating near-vertically. For larger offsets (wide angles), however, the model predicts considerably later arrival times than observed. The three other OBS, where the S_MS phase is observed for wide angles only, show the same difference between observed and calculated traveltimes.

The deviation may be partly explained by assuming a lateral variation in the crustal *S*-wave velocity. About half of the observed deviation may be explained by assuming the presence of a low *S*-wave velocity body ($V_S \approx 3.3$ km s^{-1}) in the lower crustal bulge between about 40 and 75 km offset and 14 and 18 km depth (Fig. 13) together with higher *S*-wave velocity ($V_S \approx 4.0$ km s^{-1}) elsewhere in the lower crust. Lateral variations in the *S*-wave velocity cannot, however, explain the observations satisfactorily.

Another explanation that has been investigated is the possibility that the *S*-wave Moho is not coincident with the *P*-wave Moho. Varying the depth to the *S*-wave Moho laterally can again explain about half of the observed deviation. No better fit is achieved by combining lateral variation in the *S*-wave velocity with lateral variation in the position of the *S*-wave Moho.

5.3.1 *Anisotropy in the lower crust*

The only simple explanation for the observed S_MS deviation is seismic anisotropy: the *S*-wave velocity seems to increase with increasing angle of incidence. Anisotropy is not presently incorporated in the modelling package employed, but the phenomenon can be easily studied indirectly. From OBS 7 (Fig. 10) it is found that an *S*-wave velocity of 3.5 km s^{-1} ($V_P/V_S = 1.95$) satisfies the observations for a vertically propagating *S*-wave. Fig. 14 (OBS 6) shows that the observed and calculated arrival times are the same at about 25–55 km offset when the *S*-wave velocity in the lower crust is increased to 3.8 km s^{-1} ($V_P/V_S = 1.8$). This means that an *S*-wave propagating in the lower crust with a mean incidence angle of about 30–40° propagates with a velocity of 3.8 km s^{-1}. Increasing the velocity to 4.0 km s^{-1} ($V_P/V_S = 1.7$) shows that an *S*-wave propagating in the lower crust with this velocity satisfies the observations when the mean angle of incidence is 60–70°. An *S*-wave propagating in the lower crust with an angle deviating about 60–70° from the vertical thus apparently has an approximately 14 per cent higher velocity than a vertically propagating wave.

The large apparent anisotropy is most probably restricted to the lower crust. The intercept time of the arrival from the top of the middle crust (S_{mc}) observed in OBS 6 (Fig. 7) is sensitive to the vertical *S*-wave velocity in the upper crust, and indicates that an anisotropy of this kind is not important in the upper crust. The same argument applies to the $P_MP_{lc}S$ arrival observed in OBS 7 (Fig. 10) interpreted to represent a *P*-wave that has been converted to a *S*-wave at the top of the lower crust on its way up. This arrival indicates that the

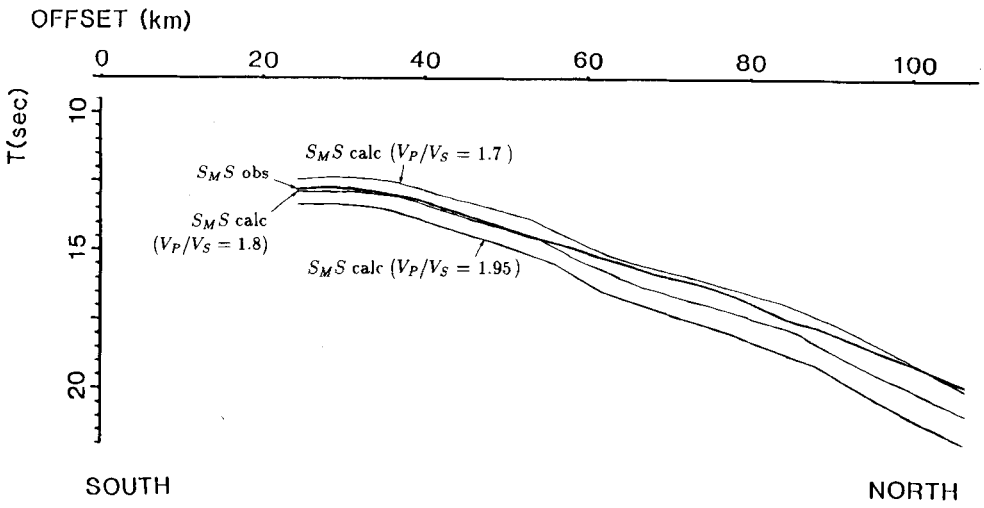

Figure 14. *S*-wave reflection from Moho observed on OBS 6 (horizontal component) compared with the calculated reflection for three different V_P/V_S ratios in the lower crust. Notice that different V_P/V_S ratios satisfy the observations for different offsets (angles of incidence).

S-wave velocity in the middle crust does not vary significantly with the angle of incidence.

The calculated P_MS arrivals (Figs 7, 10–12) deviate only to a small degree from the observed arrivals for two reasons (which follows directly from Snell's law): these arrivals propagate longer distances as *P*-waves than *S*-waves in the lower crust, and the *S*-wave part propagates nearer the vertical in the lower crust than the S_MS waves and are consequently less influenced by the anisotropy.

Numerous publications on the modelling of *S*-wave anisotropy have been published. One that seems to explain the observed anisotropy reasonably well is shown in Fig. 15 (modified from Crampin 1985). The figure shows the variation of the body wave velocities with azimuth in a solid consisting of horizontally aligned penny-shaped and saturated microcracks with a crack density (CD) of 0.1 ($CD = Na^3/v$, where N is the number of cracks of radius a and half-thickness d in volume v) and aspect ratio (AR) of 0.05 ($AR = d/a$). Crack densities of 0.1 have been estimated for some parts of the crust (Crampin 1978). The synthetic model shows that the *S*-wave velocity increases by about 10.5 per cent from vertical to 45° angle of incidence. The *P*-wave velocity decreases by about 3.5 per cent within the same range of angles. The difference between the *S*-wave and *P*-wave anisotropies, which corresponds to the anisotropy observed in OBS data, is thus 14 per cent in this example. A possible *P*-wave anisotropy of about 3.5 per cent is so small that it can hardly be revealed from the data. The *P*-wave model used as a basis for the *S*-wave modelling might thus contain a small amount of anisotropy that according to the synthetic example might increase the observed (apparent) *S*-wave anisotropy. The observed *S*-wave anisotropy of about 14 per cent might thus correspond to a real anisotropy in the order to 10 per cent.

The fact that the observed anisotropy seems to be satisfactorily explained by the synthetic modelling example described above does not imply, however, that the lower crust contains cracks. It only indicates that a model with some horizontal or subhorizontal layering (which is in accord with most models of the lower crust) and with a velocity anisotropy in the same order as in the synthetic example (which is calculated by using physically realistic parameters) seems to satisfy the observations.

The discovery of the strong anisotropy in the lower crust was made possible by the unique observation on OBS 7 (Figs 8 and 10); an *S*-wave reflection from Moho observable more or less continuously from vertical to wide-angle incidence. If the S_MS phase had been observed for wide

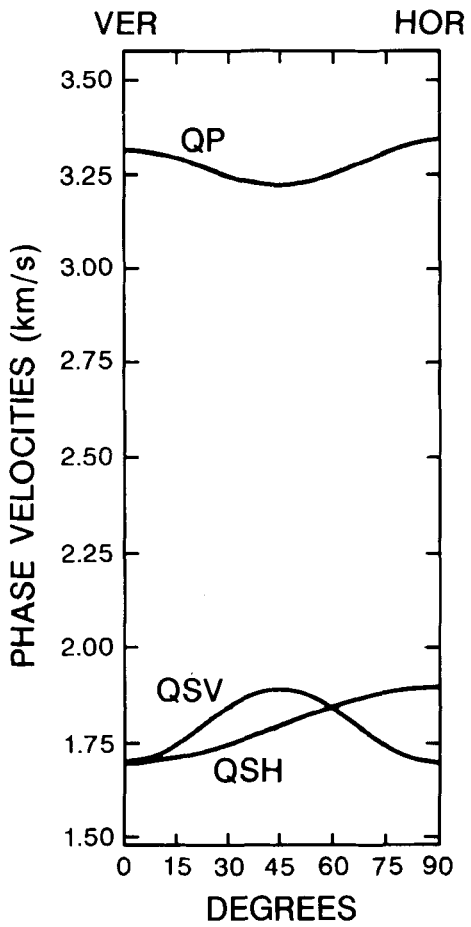

Figure 15. Variation of body wave velocities with angle of incidence in a solid consisting of horizontally aligned penny-shaped and saturated microcracks with a crack density of 0.1 and aspect ratio of 0.05. Modified from Crampin (1978).

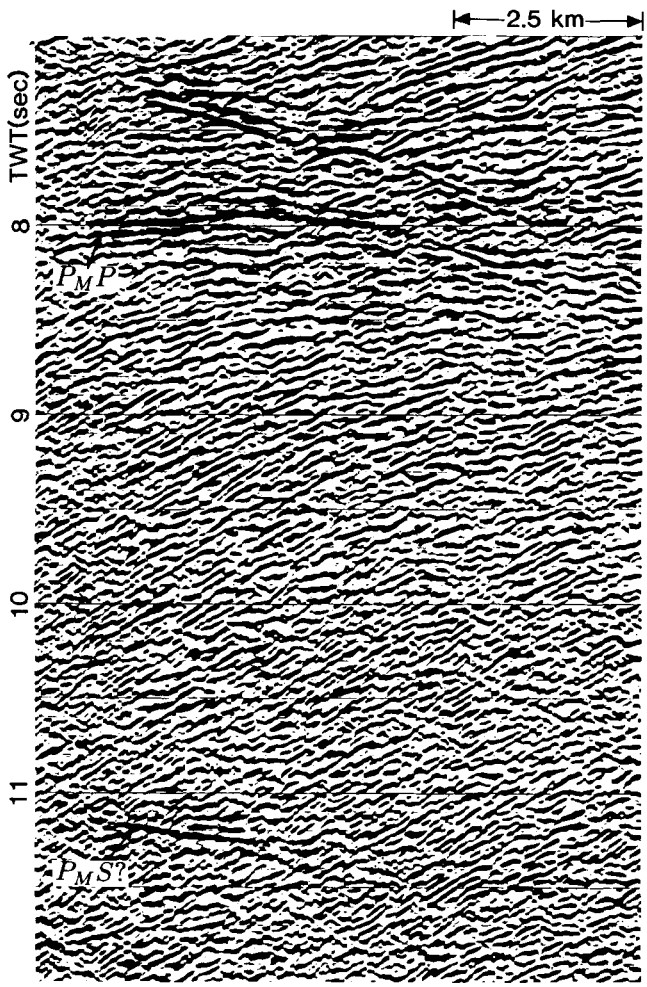

Figure 16. Part of a seismic reflection profile shot close to OBS 7 (see Fig. 1 for location). Notice the strong Moho and lower crustal reflections, and indications of a mode converted wave at Moho.

angles only in all OBS, an isotropic model with somewhat higher S-wave velocity (about 3.9 km s^{-1}; $V_P/V_S = 1.75$) in the lower crust would have satisfied the observations (see Fig. 14). The resulting deviations in the order of 500 ms in this case would have been explained by uncertainties related to the shallow structure or to the nature of Moho. The calculated V_P/V_S ratio would then have been used to put constraints on rock parameters such as lithology.

Fig. 16 shows a part of a seismic reflection line crossing the studied profile close to OBS 7 (Fig. 1). The reflection line reveals that the lower crust is highly reflective, indicating that this portion of the crust in this region consists of thin alternating high and low velocity layers probably of relatively limited lateral extent. At about 11.2 s TWT an approximately 2 km long, strong reflector is observed. Its traveltime corresponds to the vertical two-way traveltime for the P_MS arrival identified on OBS 7 and clearly observable on the vertical component (Fig. 9). This observation demonstrates that S-waves always should be kept in mind when deep crustal seismic reflection data are interpreted, particularly when 'sub-Moho reflections' are identified.

5.4 The *S*-wave model in the upper mantle

Arrivals interpreted as S_n arrivals are indicated in Figs 7, 11 and 12, and an upper mantle S-wave velocity of 5.1 km s^{-1} ($V_P/V_S = 1.6$) is estimated. The continuity in these weak arrivals is very poor, however, and this interpretation should be considered as very preliminary.

6 CONCLUSIONS

A consistent S-wave velocity model along a 145 km long profile on the Røst High off Lofoten, northern Norway, has been obtained by studying the horizontal components of four OBS. Strong crustal S-waves and P- and S-wave reflections as well as P-to-S conversions at the Moho are observed.

S-waves from the sediments and upper crystalline crust indicate that the V_P/V_S ratio in the sediments varies both vertically and laterally, which probably can be attributed to increased compaction with depth and a change in lithology from shale on the Røst High to more sandy sediments south of the High.

On one OBS the S-wave reflection from the Moho can be followed continuously from vertical to wide-angle incidence. This unique observation enables the detection of about 10 per cent S-wave anisotropy in the lower crust, consistent with some horizontal or subhorizontal layering. The presence of layering in the lower crust is also indicated from multichannel reflection seismics which reveal strong subhorizontal reflections at these depths.

The detection of the anisotropy in the lower crust shows that extreme care must be taken when the V_P/V_S ratio is interpreted in terms of lithology and other rock parameters, and that anisotropy should always be kept in mind when S-waves are studied.

ACKNOWLEDGMENTS

I thank Professor M. A. Sellevoll (Institute of Solid Earth Physics) for indispensable support throughout the work, and Professor R. Kanestrøm (Norsk Hydro and Institute of Solid Earth Physics) and Dr C. Hurich (Institute of Solid Earth Physics) for critically reading the manuscript.

I thank further Professor H. Shimamura, Dr T. Iwasaki, (Laboratory for Ocean Bottom Seismology, University of Hokkaido) and Professor T. Kanazawa, (Laboratory for Earthquake Chemistry, University of Tokyo) for providing instruments and indispensable help during the acquisition and pre-processing of the data.

I finally thank Statoil for financial support and help; in particular, I would like to thank E. W. Berg, V. B. Larsen, L. B. Pedersen and K. J. Skaar.

REFERENCES

Assumpcao, M. & Bamford, D., 1978. LISPB, V, studies of crustal S-waves, *Geophys. J. R. astr. Soc.*, **54,** 61–73.

Bøen, F., Eggen, S. & Vollset, J., 1984. Structures and basins of the margin from 62–69°N and their development, in *Petroleum Geology of the North European Margin*, pp. 3–28, eds Spencer, A. M. *et al.*, Graham and Trotman, London.

Braile, L. W., Smith, R. B., Keller, G. R., Welch, R. M. & Meyer, R. P., 1974. Crustal structure across the Wasatch Front from detailed seismic refraction studies, *J. geophys. Res.*, **79,** 2669–2677.

Bukovics, C., Shaw, N. D., Cartier, E. G. & Ziegler, P. A., 1984. Structure and development of the Mid-Norway continental margin, in *Petroleum Geology of the North European Margin*, pp. 407–423, eds Spencer, A. M. *et al.*, Graham and Trotman, London.

Christensen, N. I., 1984. Pore pressure and oceanic crustal seismic structure, *Geophys. J. R. astr. Soc.*, **79,** 411–423.

Christensen, N. I. & Fountain, D. M., 1975. Constitution of the lower continental crust based on experimental studies of seismic velocities in granulite, *Geol. Soc. Am. Bull.*, **86,** 227–236.

Chroston, P. N. & Brooks, S. G., 1989. Lower crustal seismic velocities from Lofoten–Vesterålen, north Norway, *Tectonophysics*, **157,** 251–269.

Crampin, S., 1978. Seismic wave propagation through a cracked solid: Polarization as a possible dilatancy diagnostic, *Geophys. J. R. astr. Soc.*, **53,** 467–496.

Crampin, S., 1985. S-wave propagation through real rock, *GSU Report No.* 244, 50 pp.

Crampin, S., 1990. The scattering of S-waves in the crust, *Pageoph*, **132,** 67–91.

Drivenes, G., Sellevoll, M. A., Renard, V., Avedik, F. & Pajchel, J., 1984. The continental margin/crustal structure off the Lofoten Islands, northern Norway, in *Petroleum Geology of the Northern European Margin*, pp. 211–216, eds Spencer, A. M. *et al.*, Graham and Trotman, London.

Gage, M. S. & Dore, A. G., 1986. A regional geological perspective of the Norwegian offshore exploration provinces, in *Habitat of Hydrocarbons on the Norwegian Continental Shelf*, pp. 21–38, Norwegian Petroleum Society, Graham and Trotman, London.

Gajewski, D., 1981. S- and converted waves in the interpretation of deep seismic measurements in the Kalahari craton, Namibia, *Diploma thesis*, University of Clausthal, Germany, (in German).

Gajewski, D., Strangl, R., Fuchs, K. & Sandmeier, K. J., 1990. A new constraint on the composition of the topmost continental mantle—anomalously different depth increases of P- and S-velocity, *Geophys. J. Int.*, **103,** 497–507.

Goodwin, E. B. & McCarthy, J., 1990. Composition of the lower crust in west central Arizona from three-component seismic data, *J. geophys. Res.*, **95,** 20 097–20 109.

Hall, J. & Ali, M., 1985. *S*-waves in a seismic survey of Lewisian basement: An extra control on lithological variation and porosity, *J. geol. Soc. Lond.*, **142,** 677–688.

Holbrook, W. S., Gajewski, D., Krammer, A. & Prodehl, C., 1988. An interpretation of wide-angle compressional and shear-wave data in southwest Germany: V_P/V_S ratio and petrological implications, *J. geophys. Res.*, **93,** 12 081–12 106.

Holbrook, W. S., Gajewski, D. & Prodehl, C., 1987. *S*-wave velocity and Poisson's ratio structure of the upper lithosphere in southwest Germany, *Geophys. Res. Lett.*, **14,** 231–234.

Kanestrøm, R. & Johnstad, S. E., 1975. *Crustal structure of southern Norway from* SV *and* SH *waves,* Seismological Observatory, University of Bergen.

Kern, H., 1982. Elastic wave velocity in crustal and mantle rocks at high pressure and temperature: the role of high-low quartz transition and of dehydration reactions, *Phys. Earth planet. Inter.*, **29,** 12–23.

Kullinger, B. & Lund, C. E., 1986. A preliminary interpretation of *S*-wave traveltimes from Fennolora data, *Tectonophysics,* **126,** 375–388.

Løseth, H., Hansen, J. W., Århus, N., Weiss, H. M. & Rokoengen, K., 1989. Palynological dating and organic geochemistry of bedrock samples off Lofoten and Vesterålen, *IKU report No.* 24 1504.00/0189, 27 pp.

Mjelde, R., Sellevoll, M. A., Shimamura, H., Iwasaki, T. & Kanazawa, T., 1991. A crustal study off Lofoten, N. Norway, by use of 3-component ocean bottom seismographs, *Tectonophysics,* in press.

Mokhtari, M., 1991. A geological model for the Lofoten continental margin, *submitted in partial fulfillment of the requirements for the Dr. Scient. Degree,* Univ. of Bergen.

Mokhtari, M. & Pegrum, R. M., 1991. A geological model for the Lofoten continental margin, offshore Norway, Norsk geol. tidskr., in press.

Mokhtari, M., Pegrum, R. M. & Sellevoll, M. A., 1989. A geophysical study of the Norwegian continental margin between 67°N and 69°N, *SEISMO-SERIES No. 28,* Seismological Observatory, University of Bergen, 18 pp.

Neidell, N. S., 1985. Land applications of *S*-waves, *Geophysics: The Leading Edge of Exploration,* **11,** 32–44.

Nur, A. & Simmons, G., 1969. The effect of saturation on velocity in low porosity rocks, *Earth planet. Sci. Lett.*, **7,** 183–193.

Ostrander, W. J., 1984. Plane-wave reflection coefficients for gas sands at non-normal angles of incidence, *Geophysics,* **49,** 1637–1648.

Rokoengen, K. & Sættem, J., 1983. Shallow bedrock geology and quaternary thickness off northern Helgeland, Vestfjorden and Lofoten, *IKU report No. P 155/2/83,* 44 pp.

Sellevoll, M. A., 1973. Mohorovicic discontinuity beneath Fennoscandia and adjacent parts of the Norwegian Sea and North Sea, *Tectonophysics,* **20,** 359–366.

Sellevoll, M. A. & Pomeroy, P., 1968. A traveltime study for Fennoscandia, *Årbok for Universitetet i Bergen—Mat. Naturv. Serie,* No. **9,** 29 pp.

Sellevoll, M. A. & Thanvarachorn, P., 1977. A seismic reconnaissance study of the Earth's crust in the Lofoten–Vesterålen area, northern Norway, *in The Norwegian Geotraverse Project,* pp. 101–113, ed. Heier, K. S., Norg. Geol. Unders., Trondheim.

Spencer, J. W. & Nur, A., 1976. The effect of pressure, temperature and pore water on velocities in Westerly granite, *J. geophys. Res.*, **81,** 899–904.